Diffuse retro-reflective imaging for improved mosquito tracking around human baited bednets

Vitaly Voloshin[a,*], Christian Kröner[a], Chandrabhan Seniya[a], Gregory P. D. Murray[b], Amy Guy[b], Catherine E. Towers[a], Philip J. McCall[b], and David P. Towers[a]

[a]School of Engineering, University of Warwick, Coventry, CV4 7AL, UK
[b]Liverpool School of Tropical Medicine, Pembroke Place, Liverpool, L3 5QA, UK

July 4, 2019

Abstract

Robust imaging techniques for mosquito tracking around human baited bednets are important for the development and understanding of interventions to mitigate vector-borne disease transmission. Whilst there have been recent innovations in optical imaging systems and associated signal processing, there remain issues around ease of use in the field and reliability of extracting data in the critical areas across the bednet where the optical signal is attenuated. In this paper we describe the use of a retro-reflective screen at the back of the measurement volume to simultaneously provide diffuse illumination, largely remove optical alignment issues and require only one sided access to the measurement space. Whilst the illumination becomes significantly more uniform, noise removal algorithms are needed to reduce the effects of shot noise particularly across the low intensity bednet regions. By systematically introducing mosquitoes in front and behind the bednet in lab experiments we are able to demonstrate the performance of the tracking system in these challenging areas. Overall, it is shown that the retro-reflective imaging setup can deliver mosquito segmentation rates in excess of 90% compared to less than 70% for previous back-lit systems.

Keywords: mosquito tracking, retro-reflective screen, entomology

*Corresponding author: Vitaly Voloshin, v.voloshin@warwick.ac.uk

1 Introduction

Many arthropod vectors of human infections are highly adapted to the human home and in many regions worldwide, transmission of malaria, leishmaniasis, Chagas disease, lymphatic filariasis and tick-borne relapsing fever occurs when the vectors take blood from sleeping humans. Bednets treated with insecticide can be very effective in preventing transmission of these infections and in Africa, the factory-treated durable type of nets referred to as long-lasting insecticidal nets (LLINs), are the most effective method available and an essential element of malaria control and elimination strategies today. Increased understanding of vector behaviour at LLINs, including how different LLIN treatments affect mosquito flight around and contact with the net surface is essential for understanding LLIN modes of action [1, 2] and raises the prospect of developing more effective interventions to reduce disease transmission [3, 4].

Optical imaging techniques are a natural candidate for quantifying vector behaviour given their high spatial and temporal resolution [5, 6], but their application in typical sub-Saharan Africa dwellings present particular challenges. The most important regions to target are around the sleeping space, the bednet suspended above it and the regions around this in order to examine approach and attack behaviours [7, 8]. Hence, the inspected volume ideally needs to be 2 x 2.5 x 1.5 m (depth x width x height), which easily encompasses the space around a typical installed bednet. To avoid rapidly varying spatial resolution between the front and back of the measurement volume, telecentric approaches are desirable for both illumination and imaging and given the space constraints in sub-Saharah dwellings this leads to typically 0.5 Numerical Aperture (NA) optical systems. The bednet itself is a regular grid that occludes the mosquito images – particularly as multiple layers of netting are often used. The mesh size in the bednet is typically smaller than the mosquito, *Anopheles gambiae* are 2.5 – 3.5 mm in wing length [9], hence the mosquito images are partially occluded when the mosquito is in front or behind a bednet. Furthermore, for field studies the optical system needs to be simple to setup and robust to environmental instabilities, e.g. flexible wooden floors.

Two and three dimensional (multi camera) imaging setups have been reported using illuminated diffuse surfaces or lamps as a background [10–12]. Combined with algorithms for tracking, two or three dimensional flight trajectories are produced from which responses to attractants or interventions can be determined via manual inspection. However, such analyses whilst of value, do not determine responses to an insecticide treated bednet, which

remains the most widespread and effective intervention against disease transmission [13, 14]. Field studies to examine mating behaviour have been reported using the setting sun as a back light with a pair of stereo cameras to give 3-D mosquito tracks over volumes of metre-scale dimensions [15, 16]. Large field of view back lit imaging systems have been reported with two parallel imaging channels to give a measurement volume of 2 x 2 x 1.4 m in total with large aperture Fresnel lenses enabling collimated illumination and telecentric imaging [17].

Algorithms were also reported that produced flight tracks of 25 mosquitoes over hour long recording periods [17]. Four behavioural modes were identified: swooping, visiting (the bednet), bouncing and resting. The data gave insight into mosquito host seeking behaviour and quantified an individual mosquito's contact with the bednet (and hence insecticide) [1, 2]. Despite these advances, conducting these experiments in the field is challenging. The imaging approach worked in transmission with a Fresnel lens at either end of the measurement volume, consequently 1.5 m was needed beyond the lenses at each end. The use of two Fresnel lenses per camera also generates undesirable amplitude modulation in the images in circular rings and needs very careful alignment of the two lenses with respect to each other. The unstable nature of test environments in sub-Saharan Africa dwellings means that the alignment of these large aperture Fresnel lenses needed regular adjustment.

In this paper we introduce a modified optical setup using a retro-reflective screen (RRS) to remove the optical alignment problems and also reduce the size of the optical setup. In this approach a single Fresnel lens per camera is used to both collimate the illumination and focus the light reflected from the RRS at the far end of the measurement volume. The RRS means that no further optical components are needed at one end of the measurement volume. It is found that, in transmission through a bednet, the light amplitude is reduced and in this reflective mode the light is attenuated through twice the number of bednet layers compared to the back-lit setup. Additional data processing algorithms are introduced to handle the increased range of contrast in the images. The following sections describe the optical setup and signal processing. Sets of experimental data are shown where mosquitoes are introduced into known spatial locations, e.g. in front or behind a bednet – as a means of confirming mosquito detection ability in all regions of the image. Hence, tracking performance comparisons are made between the back-lit and RRS based imaging approaches.

2 Methods

2.1 Optical Setup

The optical setup is shown in Figure 1. Light from an LED ring light expands over the Fresnel lens (approx. 1.4 x 1.0 m aperture, 1.2 m focal length) and is then approximately collimated to illuminate the space above the bednet and through the bednet itself. A volunteer acts as human bait lying beneath the bednet. The light travels to a back wall where it is reflected back via a RRS. Whilst a number of retro-reflective materials are available, improved performance was found using 3M™ Scotchlite™ High Gain 7610 [18] obtained as a tape to be stuck to the back wall. The material contains glass beads and is based on an exposed lens material, which means it does not have a glossy surface cover leaving a matt appearance and giving a 10° reflection cone. The RRS is placed approximately 2 m from the Fresnel lens. The reflected light re-crosses the measurement volume and is focused by the same Fresnel lens which forms a telecentric lens pair with an imaging optic mounted on the camera. This configuration allows illumination and imaging from one side of the bednet and scene and is relatively insensitive to alignment owing to the retro-reflective nature of the beads in the RRS.

Ideally the illuminating LED would be placed on axis along with the camera optic, however this is practically difficult owing to the high NA needed in both illumination and imaging at approximately 0.5. The LEDs are therefore positioned outside the camera optic's aperture leading to pairs of images from individual mosquitoes. A direct image of the mosquito is seen by the camera against the bright RRS and a shadow image is formed from the slightly off-axis LED on the RRS [19]. For 2D tracking over the 2 m depth of field needed here only the direct image is required. The contrast of the direct image is higher than that of the shadow images due to the extended distance over which diffraction occurs for the latter. Furthermore, each LED within the ring light will form shadows in different spatial locations of the image, whereas the direct image is in the same location and becomes reinforced with each additional LED. A custom ring light source was constructed with 12 OSRAM™ SFH 4235 infrared LEDs (peak wavelength 850 nm) [20]. The wavelength provides good sensitivity for monochrome silicon based detectors and there is no evidence from previous back-lit experiments that the direction of the illumination and orientation of the human bait affected mosquito behaviour [1, 5].

The inset in Figure 1 shows a photograph of the ring light and mounting arrangement

via an optical rail that allows independent adjustment of LED plane with respect to the camera. RRS based imaging experiments were conducted with 12 MPixel cameras, either Ximea CB120RG-CM or Dalsa FA-80-12M1H, operating at 50 fps and with 14 mm focal length camera lenses. The optical system is approximately telecentric, with the deviations coming from the steps in the Fresnel lens (which makes such a large aperture lens physically manageable) and the RRS which gives a cone of reflected light, partly compensated by closing the camera lens aperture to typically F8.0. The lens combination gives approximately 0.5 mm per pixel which gives adequate sampling of the *Anopheles gambiae* mosquito which is typically 2.5-3.5 mm wing length (other species can be much larger). Hence, in the images there is a bright background with the mosquitoes appearing as dark shadows. In the RRS approach there is a double pass of the measurement volume giving increased diffraction which limits the practical depth of field to approximately 2 m.

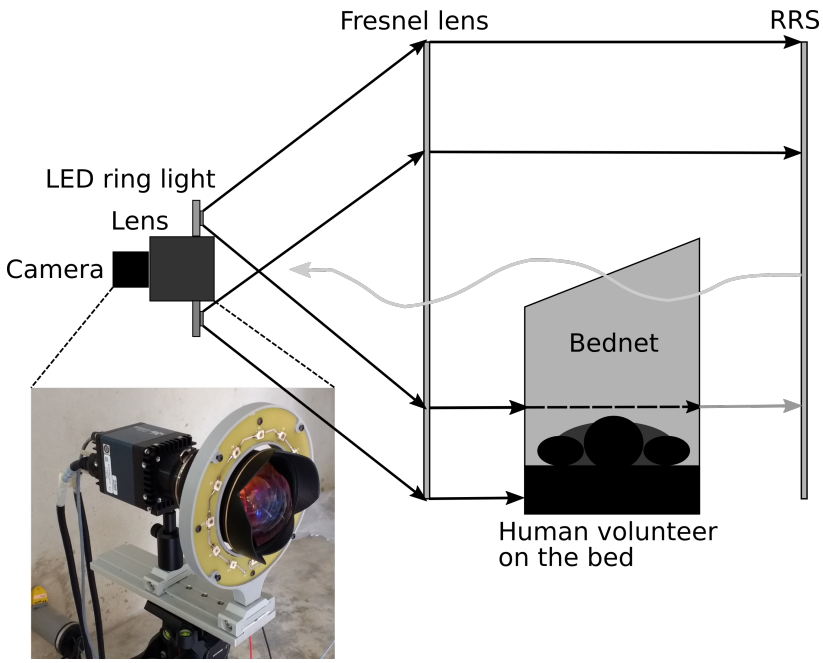

Figure 1: Schematic diagram of the recording system. Inset photograph of the ring light mounted together with the camera on a standard photographic tripod.

2.2 Signal Processing

In order to interpret mosquito behaviours it is imperative to be able to track them when swooping above or around the bednet as well as when host seeking and probing the net.

To form contiguous tracks across all the different areas, a robust segmentation process is needed. When the mosquitoes are in the region above the bednet there is at least 3-5 greyscales difference between the mosquito image and the background. The contrast reduces markedly when the mosquito is either in front or behind the bednet. With the RRS setup the light passes each layer of the bednet twice (see Figure 1) leading to 2-3 greyscales difference between the mosquito and background when the mosquito is in front of the net (closer to the Fresnel lens) and about 1-2 greyscales for mosquitoes behind the net. Graphs of the intensity distribution around a mosquito image are given in Figure 2 in both 3D (inverted intensity scale) and image formats. Figure 2a shows a mosquito shadow image using back-lit imaging when the mosquito is outside the bednet, the corresponding image with RRS imaging is in Figure 2b. Significantly reduced contrast can be seen in Figure 2c which is a back-lit mosquito image from in front of the bednet and Figure 2d from the RRS approach.

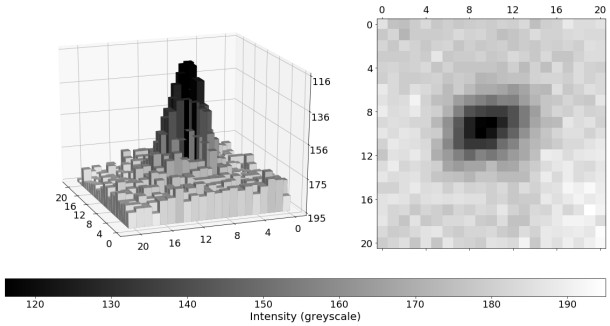

(a) Back-lit illumination, mosquito above the bednet

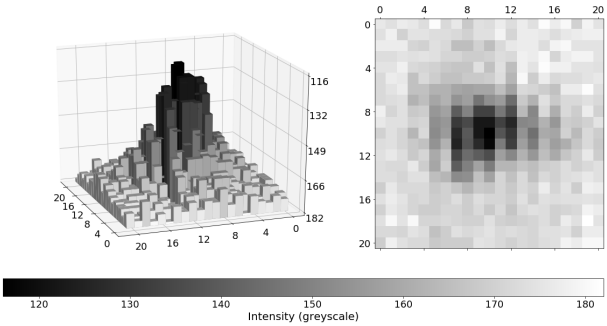

(b) RRS illumination, mosquito above the bednet

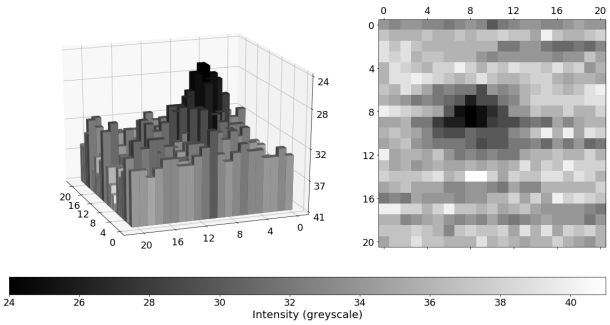

(c) Back-lit illumination, mosquito in front of bednet

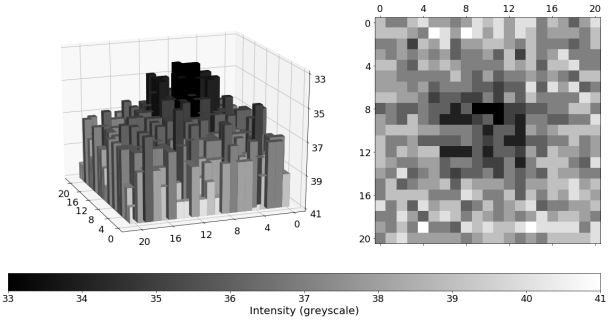

(d) RRS illumination, mosquito in front of bednet

Figure 2: Mosquito intensity distributions under back-lit or RRS illumination and for mosquito positions above the bednet or in front of the bednet. 3D maps use inverted intensity scale.

The previous approach to segmentation [17] used a difference image between consecutive frames and a single threshold value to identify movement and was found to give either too many false positive mosquitoes (from camera noise, threshold too low) or insufficient detections across the bednet (threshold too high). Particularly in low intensity regions over the bednet, the camera noise levels are similar to the contrast found across a mosquito image. A Gaussian filter is introduced to reduce noise levels in the difference image using a 15 x 15 pixel kernel and the width of the Gaussian function defined by the standard deviation as [21]

$$\sigma = 0.3 \cdot ((ksize - 1) \cdot 0.5 - 1) + 0.8.$$

The filter values were scaled such that the integral across the whole filter was 1. The benefit of the filter can be observed in Figure 3 which shows as red the pixels above a user defined threshold before and after application of the filter, in this example the threshold was 2 greyscales.

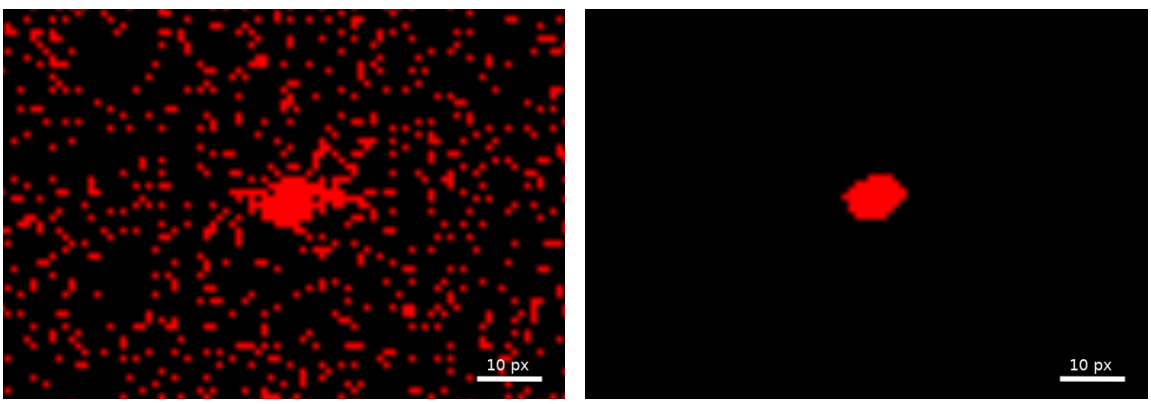

(a) Image before denoising applied.

(b) Image after de-noising, 15 x 15 pixel Gaussian filter, standard deviation 2.6.

Figure 3: The effect of de-noising on part of a difference image containing a mosquito image. Both cases show the same part of the frame. The red colour shows differences greater than 2 greyscales.

A normalised histogram from the RRS system shows the greyscale ranges associated with the different regions of the image, see Figure 4b. The two regions of interest for mosquito flight are the background which is above or to the side of the bednet and the bednet region itself, either in front or behind the bednet. A manual definition of the threshold that separates these regions is required to run segmentation algorithm and is typically around 40-60 greyscales and is consistent for both backlit and RRS imaging approaches. It can be seen from Figure

4 that the RRS system gives larger regions of high intensity in the background whereas this region is more widely distributed for the backlit case. The bednet region has a larger greyscale range for the backlit system (showing less uniform illumination in the backlit case), but its peak is at a higher greyscale, approximately 40, than for the RRS system. It can also be seen that the darkest regions, corresponding to the human bait are brighter for the RRS by circa 10 greyscales than in the backlit case. This occurs due to the direct front illumination which will also be incident on the mosquitoes and reduce the contrast in comparison with the background.

The segmentation algorithm reported here incorporates the following stages.

1. Form a difference image between the nth and (n-i)th images. Typically i is set to 5 frames to aid discrimination. This produces a pair of detected images with opposite signs and their separation is the mosquito displacement between the two frames.

2. A large kernel, typically 9 x 9 to 21 x 21 pixel, Gaussian filter is then (optionally) applied to the difference image to reduce noise.

3. For the brighter, background region, the algorithm searches for all regions of positive difference. An image threshold is calculated and applied to segment the mosquito image. Morphological operators can be optionally applied to improve the outer contour of the mosquito image (opening and closing). Statistics are then calculated: the centre co-ordinates, the area, i.e. standard 'blob' analysis. Dilation performed by 5-7 pixels aid the detection of broken down images. Mosquito images are removed with either too large or small area (based on user defined thresholds). The result is a set of candidate mosquito images that satisfy the selection criteria and their positions in the image.

4. The process is repeated for the darker image regions containing the bednet. The threshold used to segment the mosquito images tends to be lower at 1 to 2 greyscales.

5. The data from the two passes (the brighter and darker image regions) are then combined together.

Besides Gaussian filter for de-noising (OpenCV library was used for implementation [21]), the mosquito segmentation algorithm is identical to the one described in [17]. Originally, the algorithm was used in a single pass, whereas here the image is split into two regions by simple intensity threshold and each region is passed by the segmentation algorithm separately.

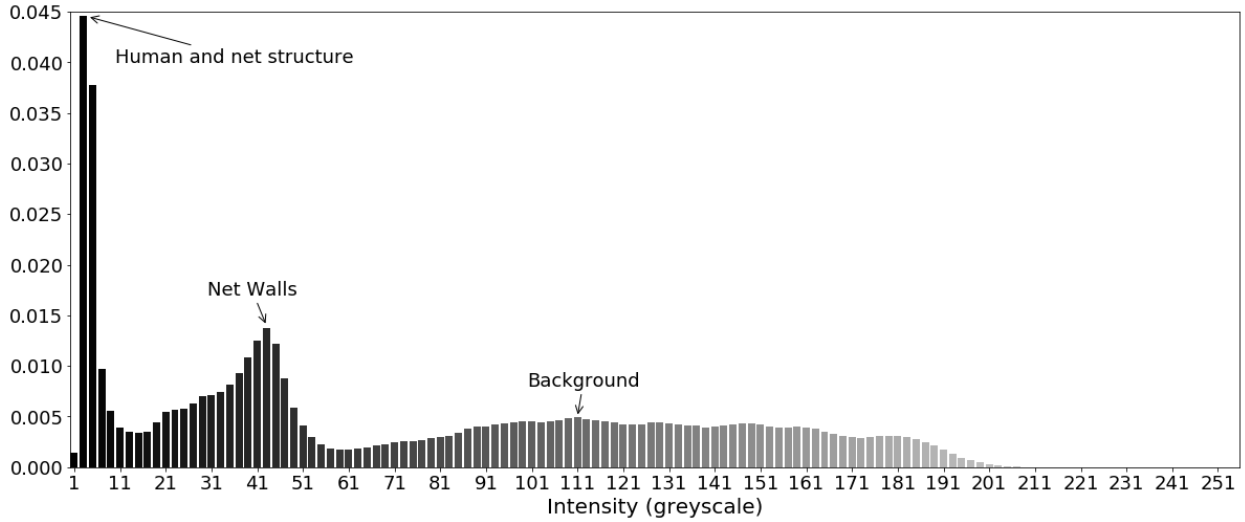

(a) Back-lit image histogram

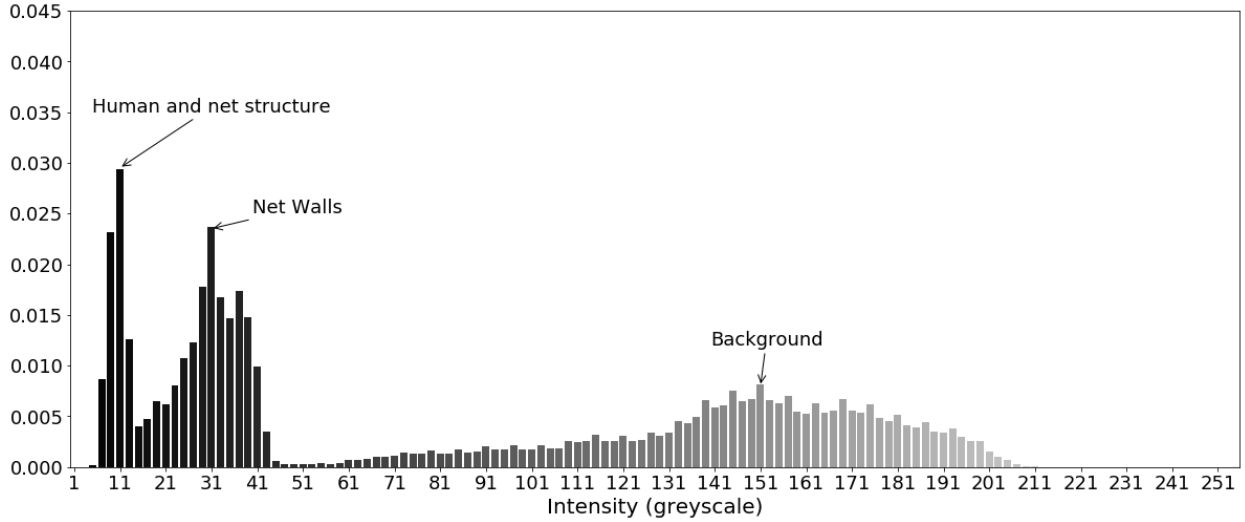

(b) RRS image histogram

Figure 4: Normalised image histograms with different illumination approaches.

3 Results and discussion

3.1 Evaluation of Illumination quality

Exemplar images from the backlit and RRS illumination systems are given in Figure 5. The ring structure from the pair of Fresnel lenses used in the backlit approach are visible across

the image in Figure 5a, whereas this structure is averaged out when a single Fresnel lens is used with the RRS in Figure 5b. The horizontal banding in the RRS image derives from the 50 mm wide adhesive tape obtained from 3M and the reflections from the LED ringlight give small localised areas where individual mosquito images cannot be segmented. In the backlit case the roof of the bednet is tilted whereas with RRS these data were obtained using a flat bednet roof. Each figure shows 3 intensity profile graphs in the region above the bednet, i.e. the background. It can be observed that with the RRS the intensity towards the edge and corners of the image is maintained at a higher level, whereas with backlit imaging the intensity drops to <50% of the central area. The ring structure from the two Fresnel lenses can also be seen in the profiles from Figure 5a with backlit imaging and for unstable field recordings can lead to erroneous artefacts in the difference images used for mosquito segmentation.

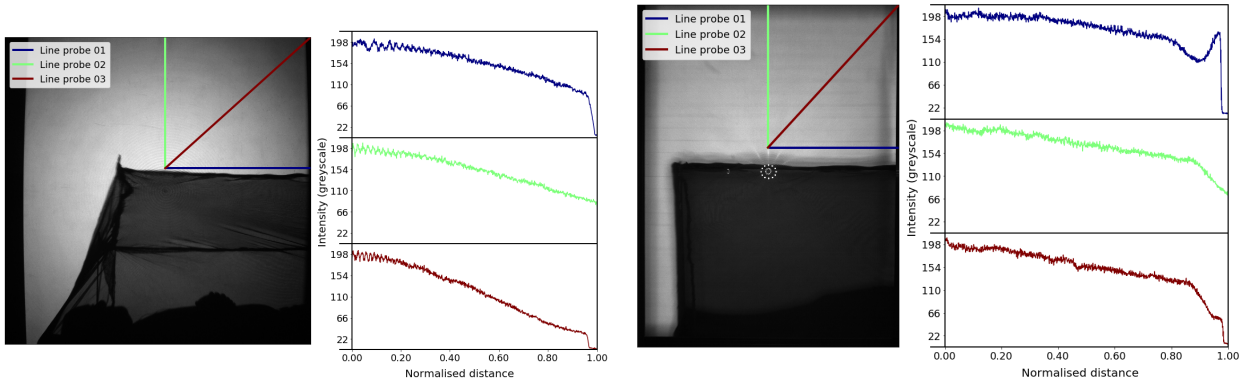

(a) Image from backlit system

(b) Image from retroreflective screen system

Figure 5: Spatial distribution of light levels across the background of the image along three different directions using line probes. Line probes are parameterised by a coordinate from 0 to 1, where 0 is at the centre of the image and 1 is at the edge.

The temporal stability of the illumination using the bespoke LED ring light source was compared with that of the original single LED used in the original backlit system. Statistical analysis over 250 frames (5 seconds) of data in different parts of the image showed the expected result that the standard deviation and greyscale range increase with mean intensity. The cameras used for backlit imaging and those in the RRS experiments both using the same type of CMOSIS detectors and gave average levels of 1.84% greyscale standard deviation as a proportion of the mean intensity.

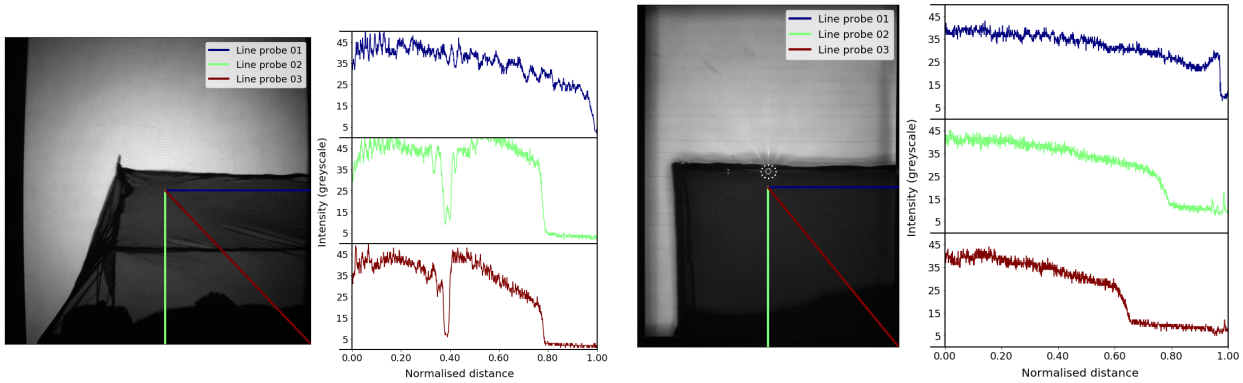

(a) Image from backlit system

(b) Image from retroreflective screen system

Figure 6: Spatial distribution of light levels across the bednet along three different directions using line probes. Line probes are parameterised by a coordinate from 0 to 1, where 0 is at the centre of the image and 1 is at the edge.

3.2 Quantitative performance metrics

The performance of the combined imaging and segmentation algorithms has been quantified using a number of metrics, thus enabling a quantitative comparison of the backlit and RRS imaging setups. The data are presented in Table 1. Each dataset was obtained from a typical 1 hour recording with the cameras operating at 50 frames per second. The image sequences were segmented using the algorithm described above with the parameters optimised for each dataset. Notably, the greyscale threshold for detection of mosquito images across the challenging bednet region was the same (1 greyscale). An initial tracking process was performed [17] allowing only a single missing mosquito position within a track and discarding any tracks with less than 5 positions; hence the number of 'detected positions in tracks' in Table 1 is determined. A second tracking iteration enabled existing tracks to be lengthened and tracks to be combined together with gaps of up to 15 frames between consecutive positions in a track.

Any gaps in a track, i.e. where the time between consecutive track positions is a multiple of the inter-frame time, Δt, indicate a missed mosquito position. Some missed positions occur as mosquitoes fly across completely occluded areas but others are due to locally poor

contrast. The total number of potential positions in a track, N_t, is calculated from:

$$N_t = \sum_{k=0}^{n-1} \texttt{Int}\left[\frac{\Delta t_k}{\Delta t}\right],$$

where n - number of recorded positions, Δt_k - time difference between the current and previous recorded position, $\texttt{Int}[\ldots]$ gives the nearest integer value. An individual gap in a track is identified when $\texttt{Int}\left[\frac{\Delta t_k}{\Delta t} - 1\right] > 0$ and hence the total length of gaps in a track, N_{Gaps}, is given by:

$$N_{Gaps} = \sum_{k=0}^{n-1} \texttt{Int}\left[\frac{\Delta t_k}{\Delta t} - 1\right],$$

The data in Table 1 provides average and standard deviation of gap size as well as the number of gaps as a proportion of the number of detected positions (to normalise the expected experimental variability). These metrics are determined for the background (outside the bednet) and the across the bednet regions. Statistics are also given for the average track length and average track length without gaps. The latter is the average length of track pieces without any gaps, i.e. where there is a detected position at every time step. Finally, mosquito detection percentages are given from the ratio between number of detected positions used in tracks and total number of potential positions, N_t.

3.3 Discussion

The rationale for the RRS based imaging system has been described above and it is clear that this approach delivers a smaller operational footprint as well as only needing optical access from one side of the measurement volume. It is worth noting that the backlit system has a very small optical power density where the scene volume was 4.8 m^3 and total light source power output is 0.88 W (for two LEDs), thus, light power density is 0.18 W/m^3. The new system provides slightly larger scene volume (due to greater height of the Fresnel lenses) of 5.9 m^3, but light source power output is approx. 12 W (for two LED ring lights) and, thus, the optical power density is 2 W/m^3. Repeat experiments and rotation of the human bait show that the increased power density from the fixed position of the illumination does not influence the behaviour of the mosquitoes. There are additional benefits in uniformity of

[1]Retroreflective screen system

Table 1: Performance metrics of mosquito position detection for backlit and retroreflective screen systems.

Metrics \ Systems	Backlit [17]	RRS[1]
Detected positions in Tracks	19128	22483
Mean ± SD Gap Size (Frames) Across Net	6.88 ± 11.91	4.19 ± 4.22
Gaps/Positions Ratio Across Net	0.066	0.018
Mean ± SD Gap Size (Frames) Outside Net	4.18 ± 6.58	4.58 ± 4.62
Gaps/Positions Ratio Outside Net	0.036	0.017
Average Track Length	78.02	77.54
Average Uninterrupted Track Length	16.82	29.85
Detected Mosquitoes Across Net	54%	92%
Detected Mosquitoes Outside Net	85%	92%
Detected Mosquitoes Overall	69%	92%

the illumination into the corners of the measurement volume compared to the backlit setup as evidenced by the spatial distribution data in Figures 5 and 6. There is the opportunity with more uniform illumination from RRS imaging to raise the light level further without causing saturation of the image in the centre. The practical benefits are important for ease of use in field settings, e.g. in Banfora, Burkina Faso. The RRS approach requires 2 Fresnel lenses (rather than 4 for the backlit case) and two tripods for the camera-LED assemblies (4 tripods for two cameras and two light sources for backlit). The RRS itself can be assembled in the field from locally sourced plywood sheets and the retro-reflective tape bonded to it.

The performance of the RRS approach to track mosquitoes in front of and behind the bednet has been evaluated in lab experiments where the mosquitoes are released via an aspirator at the specific locations. Segmented and tracked results are given in Figure 7a when the mosquitoes are released in front of the bednet and in Figure 7b where the point of release is behind the bednet. The image of the aspirator at the moment of release is clearly visible on the right edge of each image. Several mosquitoes were released simultaneously in each case. It is clear, that mosquitoes located closer to the Fresnel lens (in front of the net) are reliably identified by the segmentation algorithm everywhere – the tracks show a regular spacing of segmented positions. Mosquitoes flying closer to the retroreflective screen (behind the net) are consistently identified above the net and across the vertical net walls. Segmentation

performance is slightly worse across the inclined net roof, although most positions are still identified and sufficient to enable flight path tracking. This occurs due to the combination of limited depth of field and additional optical attenuation through the inclined net which gives increased occlusion. Also, at the beginning of the tracks mosquitoes were not identified well because they were blown from the aspirator quite fast (much faster than their natural maximum velocity).

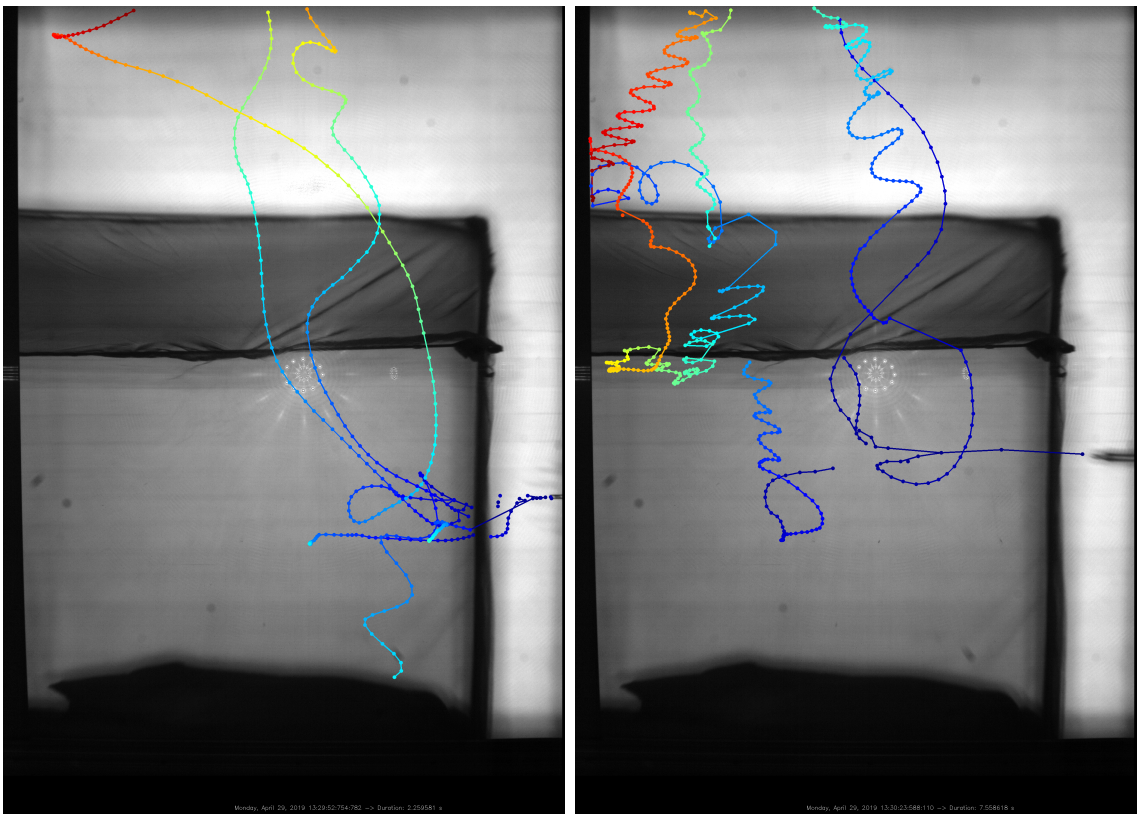

(a) Positions and tracks of mosquitoes flying in front of the bednet.

(b) Positions and tracks of mosquitoes flying behind the bednet.

Figure 7: Segmented positions of the mosquitoes and flight tracks released using an aspirator (visible on the right of each frame) specifically in front (a) and behind (b) the bednet.

Figure 8 shows identified mosquito positions from both cameras with a human volunteer lying under the net. Qualitative inspection reveals a high level of activity in front and behind the bednet as well as bouncing behaviours particularly evident above the feet of the person (left hand side but with some continuity to the right hand camera view). These data were obtained with Ximea CB120RG-CM cameras. The left hand camera used 5 ms

exposure time with 0 gain, whereas the right hand camera was used with 5 ms exposure and -3.5 dB gain. The continuity of tracks between the two views reflects the robustness of the segmentation algorithm to these varying conditions. Movement of the volunteer and draughts cause movement of the bednet and the associated strings supporting it and lead to some false segmentation in individual frames that are largely filtered out via the tracking algorithms. Supplementary video file demonstrates short part of the recording, where mosquitoes move from one side to the other and some bouncing activity on the roof of the net.

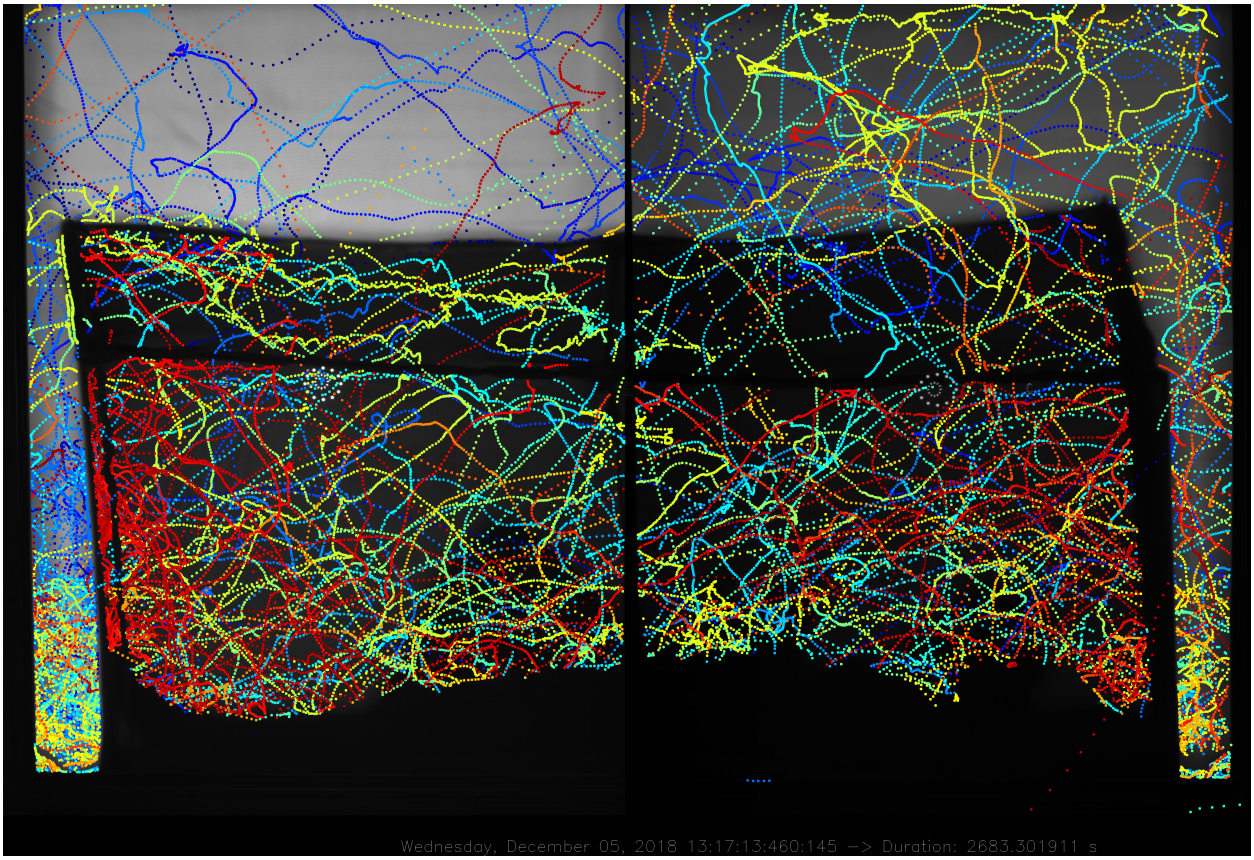

Figure 8: Example of full RRS system segmented recordings using Ximea CB120RG-CM cameras and 5 ms exposure per frame. Left camera 0 gain, right camera -3.5 dB gain.

The quantitative performance metrics presented in Table 1 are from different experiments for the backlit and RRS imaging systems and hence exhibit natural variability due to the use of different mosquitoes and human bait. This is evident in the detected positions in tracks metric which shows that the RRS experiment produced a higher number of segmented mosquito positions that passed the consistency requirements to be part of mosquito flight

tracks. The data on gap size in tracks shows that the RRS imaging approach gave similar performance both across net and outside net regions. In contrast the backlit imaging setup gives larger track gaps across the bednet probably due to reduced illumination levels away from the centre of each camera's field of view and the reduced transmission of the bednet in this region. The variability in gap size (given by the standard deviation, SD) is higher for both regions with backlit imaging, but especially so for the across net region. The data for the number of track gaps normalised by the number of detected positions shows similar trends: consistent performance from the RRS setup in both across net and outside net regions, but worse metrics with backlit imaging.

The track length data shows that average performance of backlit and RRS imaging systems is similar. However, the uninterrupted track length is significantly better for RRS than backlit, indicating the greater consistency in segmenting mosquito positions. The mosquito detection percentages show that the RRS imaging approach achieves consistent performance in both across net and outside net regions with detection levels >90% that are significantly higher than for backlit imaging. With this improved performance in mosquito image segmentation, the tracking algorithms are able to reliably bridge the gaps in tracks that do occur and hence deliver significantly improved flight tracks for entomologists.

4 Conclusions

The introduction of a retro-reflective screen to large volume, human baited mosquito tracking studies delivers significant improvements to mosquito detection rates in comparison to previous backlit imaging approaches. This is primarily due to increased uniformity of illumination and the narrow angle diffuse nature of the reflected light from the RRS. A disadvantage of RRS imaging is that the light double passes each bednet layer that is typically the focus of the experiments, reducing the available light intensity. However, the use of large kernel Gaussian noise reduction filters combined with low detection thresholds of 1 to 2 greyscales have been shown to give robust mosquito detection. With RRS imaging, mosquito detection rates of 92% have been obtained, compared to an average of 69% with backlit imaging.

There are further practical benefits of the RRS imaging setup in terms of reduced footprint, reduced number of optical components required and reduced sensitivity to mis-alignment due to the retro-reflective nature of the material. RRS based imaging setups are now in routine use for laboratory evaluation of mosquito behaviour around human baited bednets

as well as in the field, for example, at Banfora, Burkina Faso.

Acknowledgements

The authors would like to thank the volunteer sleepers both in the laboratory in Liverpool and in the field in Burkina Faso and are especially grateful to the community at Tengrela, Burkina Faso, who continue to support studies at their village.

Ethics

All research methods were performed in accordance with approved guidelines for those procedures and written informed consent was obtained from all volunteer subjects. Video recording work was approved by the Research Ethics Committees at the Liverpool School of Tropical Medicine (LSTM Research Protocol 16-38, 11 October 2016, Liverpool) and Centre National de Recherche et de Formation sur le Paludisme (CNRFP Deliberation no. 2016-9-097, 20 September 2016, Ouagadougou). No adverse effects of treatment or mosquito-borne infections were reported by volunteers during the course of the study.

Data, code and material

All custom codes (not already published elsewhere) and all data used in this work are available at [22] and larger datasets used for illumination analysis are availabe at [23].

Competing interests

The authors declare no competing interests.

Funding

This research was supported with funding from the UK Medical Research Council (MRC) and the UK Department for International Development (DFID) under the MRC/DFID Concordat agreement (MR/M011941/1), a Wellcome Trust Collaborative Award (Malaria in Insecticide Resistant Africa MiRA; 200222/Z/15/Z) and the Bill & Melinda Gates Foundation (OPP1159078).

Authors contributions

C.K., D.P.T., C.E.T. and V.V. conceived the idea of the improved system. V.V., C.K. and C.S. developed the new system and did initial testing. P.J.M. and G.M. gave advice on specifics of entomological use and field conditions for the system. G.M. and V.V. setup both field and lab based systems and did initial testing of the system at the field site. G.M. collected field test data, whereas A.G. collected test data from lab based system. C.K., C.S., and V.V. did initial pre-processing and initial assessment of the collected data. V.V. together with C.K., C.E.T., and D.P.T. developed and implemented assessment metrics and methods. C.K. with the help of C.S., C.E.T., D.P.T., and V.V. devised and implemented improvements to the segmentation algorithm. V.V. with the help of C.K. and C.S. ran the performance analysis. V.V., C.K., C.E.T and D.P.T. wrote the paper. All authors approved the final submitted version.

References

[1] J. E. A. Parker, N. Angarita-Jaimes, M. Abe, C. E. Towers, D. Towers, and P. J. McCall. Infrared video tracking of anopheles gambiae at insecticide-treated bed nets reveals rapid decisive impact after brief localised net contact. *Sci Rep*, 5, 2015. doi: 10.1038/srep13392. URL `https://doi.org/10.1038/srep13392`.

[2] J. E. A. Parker, N. C. Angarita Jaimes, K. Gleave, F. Mashauri, M. Abe, J. Martine, and C. E. Towers. Host-seeking activity of a tanzanian population of anopheles arabiensis at an insecticide treated bed net. *Malar J*, 16, 2017. doi: 10.1186/s12936-017-1909-6. URL `https://doi.org/10.1186/s12936-017-1909-6`.

[3] The malERA Consultative Group on Vector Control. A research agenda for malaria eradication: Vector control. *PLOS Medicine*, 8(1):1–8, 01 2011. doi: 10.1371/journal.pmed.1000401. URL https://doi.org/10.1371/journal.pmed.1000401.

[4] Gregory P. D. Murray, Natalie Lissenden, Jeff Jones, Vitaly Voloshin, K. Hyacinthe Toé, Ellie Sherrard-Smith, Geraldine M. Foster, Thomas S. Churcher, Josephine E. A. Parker, Catherine E. Towers, Sagnon N'Falé, Hilary Ranson, David Towers, and Philip J. McCall. Barrier bednets target malaria vectors and increase insecticide options for managing resistance. *Nature Microbiology*, Submitted, 2019.

[5] G. Gibson. A behavioural test of the sensitivity of a nocturnal mosquito, anopheles gambiae, to dim white, red and infra-red light. *Physiol Entomol*, 20, 1995. doi: 10.1111/j.1365-3032.1995.tb00005.x. URL https://doi.org/10.1111/j.1365-3032.1995.tb00005.x.

[6] Jeroen Spitzen and Willem Takken. Keeping track of mosquitoes: a review of tools to track, record and analyse mosquito flight. *Parasites & Vectors*, 11(1):123, Mar 2018. ISSN 1756-3305. doi: 10.1186/s13071-018-2735-6. URL https://doi.org/10.1186/s13071-018-2735-6.

[7] Bernadette Huho, Olivier Briët, Aklilu Seyoum, Chadwick Sikaala, Nabie Bayoh, John Gimnig, Fredros Okumu, Diadier Diallo, Salim Abdulla, Thomas Smith, and Gerry Killeen. Consistently high estimates for the proportion of human exposure to malaria vector populations occurring indoors in rural Africa. *International Journal of Epidemiology*, 42(1):235–247, 02 2013. doi: 10.1093/ije/dys214. URL https://doi.org/10.1093/ije/dys214.

[8] M. Nabie Bayoh, Edward D. Walker, Jackline Kosgei, Maurice Ombok, George B. Olang, Andrew K. Githeko, Gerry F. Killeen, Peter Otieno, Meghna Desai, Neil F. Lobo, John M. Vulule, Mary J. Hamel, Simon Kariuki, and John E. Gimnig. Persistently high estimates of late night, indoor exposure to malaria vectors despite high coverage of insecticide treated nets. *Parasites & Vectors*, 7(1):380, Aug 2014. doi: 10.1186/1756-3305-7-380. URL https://doi.org/10.1186/1756-3305-7-380.

[9] W. Takken, M. J. Klowden, and G. M. Chambers. Articles: Effect of Body Size on Host Seeking and Blood Meal Utilization in Anopheles gambiae sensu stricto (Diptera: Culicidae): the Disadvantage of Being Small. *Journal of Medical Entomology*, 35(5):

639–645, 09 1998. doi: 10.1093/jmedent/35.5.639. URL https://doi.org/10.1093/jmedent/35.5.639.

[10] S. Butail, N. Manoukis, M. Diallo, J. M. Ribeiro, T. Lehmann, and D. A. Paley. Reconstructing the flight kinematics of swarming and mating in wild mosquitoes. *J R Soc Interface*, 9, 2012. doi: 10.1098/rsif.2012.0150. URL https://doi.org/10.1098/rsif.2012.0150.

[11] Nicholas C. Manoukis, Sachit Butail, Moussa Diallo, José M.C. Ribeiro, and Derek A. Paley. Stereoscopic video analysis of anopheles gambiae behavior in the field: Challenges and opportunities. *Acta Tropica*, 132:S80 – S85, 2014. doi: https://doi.org/10.1016/j.actatropica.2013.06.021. URL http://www.sciencedirect.com/science/article/pii/S0001706X13001769.

[12] F. Hawkes and G. Gibson. Seeing is believing: the nocturnal malarial mosquito anopheles coluzzii responds to visual host-cues when odour indicates a host is nearby. *Parasit Vectors*, 9, 2016. doi: 10.1186/s13071-016-1609-z. URL https://doi.org/10.1186/s13071-016-1609-z.

[13] *World Health Organisation: World Malaria Report, WHO, Geneva*, November 2018. URL https://www.who.int/malaria/publications/world-malaria-report-2018/en/.

[14] *Back Malaria Partnership. Global Malaria Action Plan, WHO, Geneva*, 2008. URL http://archiverbm.rollbackmalaria.org/gmap/gmap.pdf.

[15] Sachit Butail, Nicholas Manoukis, Moussa Diallo, Alpha S. Yaro, Adama Dao, Sekou F. Traoré, José M. Ribeiro, Tovi Lehmann, , and Derek A. Paley. 3d tracking of mating events in wild swarms of the malaria mosquito anopheles gambiae. *Conf Proc IEEE Eng Med Biol Soc.*, 2011. doi: 10.1109/IEMBS.2011.6090163.

[16] S. Butail, N. C. Manoukis, M. Diallo, J. M. C. Ribeiro, and D. A. Paley. The dance of male anopheles gambiae in wild mating swarms. *J Med Entomol*, 50, 2013. doi: 10.1603/ME12251. URL https://doi.org/10.1603/ME12251.

[17] N. C. Angarita-Jaimes, J. E. A. Parker, M. Abe, F. Mashauri, J. Martine, and C. E. Towers. A novel video-tracking system to quantify the behaviour of nocturnal mosquitoes attacking human hosts in the field. *J R Soc Interface*, 13, 2016. doi: 10.1098/rsif.2015.0974. URL https://doi.org/10.1098/rsif.2015.0974.

[18] *3M^{TM} ScotchLite^{TM} High Gain Reflective Sheeting*, 2015. URL http://multimedia.3m.com/mws/media/1047216O/3m-scotchlite-high-grain-reflective-sheeting-7610.pdf.

[19] Kröner C, Towers CE, Angarita-Jaimes N, Parker JEA, McCall P, and Towers DP. 3d tracking of mosquitoes: A field compatible technique to understand malaria vector behaviour, 2016. Heidelberg, Germany.

[20] *OSRAM^{TM} Platinum DRAGON®, SFH 4235*, 2018. URL https://www.osram.com/ecat/Platinum%20DRAGON%c2%ae%20SFH%204235/com/en/class_pim_web_catalog_103489/global/prd_pim_device_2219732/.

[21] G. Bradski. The OpenCV Library. *Dr. Dobb's Journal of Software Tools*, 2000.

[22] *Github repository with all custom code and data*. URL https://github.com/Pigrenok/TrackingPerformance.

[23] *Two StreamPix Sequence v.5 files, which contains dataset used for illumination analysis*. doi: 10.6084/m9.figshare.8534057.